J Mater Sci (2011) 46:6656–6663
DOI 10.1007/s10853-011-5618-1

Poly(vinylidene fluoride)/poly(methyl methacrylate)/TiO_2 blown films: preparation and surface study

Weihua Tang · Tiange Zhu · Peipei Zhou · Wei Zhao · Qian Wang · Gang Feng · Huilin Yuan

Received: 5 March 2011 / Accepted: 9 May 2011 / Published online: 19 May 2011

Abstract Blown films of poly(vinylidene fluoride) (PVDF) and poly(methyl methacrylate) (PMMA) blends and PVDF/PMMA/TiO_2 composites were prepared by melting-extrusion for the first time. The crystalline structure and surface morphology PVDF/PMMA (DFMA) blown films were investigated using differential scanning calorimeter (DSC), atomic force microscope (AFM), and X-ray diffractometry (XRD). PVDF/PMMA/TiO_2 blown films were further prepared and underwent surface treatment. The results show that PVDF/PMMA/TiO_2 blown films present good mechanical properties, and acrylic acid surface-grafted films exhibit good adhesion capability and long-lasting hydrophilicity, making them attractive as encapsulation materials.

Introduction

Poly(vinylidene fluoride) (PVDF), as an industrially important semi-crystalline polymer, has found ever-increasing applications in electronics with its outstanding electric and mechanical properties [1] and ultrafiltration membrane with its excellent chemical resistance [2–4]. PVDF has a complex crystalline polymorphism with four known polymorphs called α, β, γ, and δ [5]. The α-polymorph is regarded as the most thermodynamically stable structure of PVDF and the rest three can be obtained at different solution-casting conditions and polymer blends. The crystalline structure of solution-casting PVDF films is strongly dependant on the solution crystallization temperature [6], casting solvent, blending partner polymer, and casting substrate [7–9]. When harvesting polymorph of PVDF from melt, α-polymorph monoclinic unit cell is most often obtained as the most thermodynamically stable form [1]. And β-phase PVDF, commonly used for pyro- and piezoelectric applications, is generally obtained by drawing the α-phase PVDF films at temperature range 70–87 °C [10, 11].

Besides high crystallinity, low surface tension also limits PVDF films' application in ultrafiltration membrane and various optoelectronics, especially backing sheet and encapsulating films for Si-based solar cells. For these purpose, PVDF is blended with oxygen-containing hydrophilic polymers to achieve polymer blends with the desired mechanical strength, hydrophilicity, and electric properties [12–16]. The compatibility in these polymer blends is achieved via the formation of quasi-hydrogen bonding between fluorine atoms (from PVDF) and carbonyl groups of the partner polymer [14]. Such PVDF blends reported so far include PVDF/poly(vinylpyrrolidone) (PVP) [17], PVDF/poly(ethylene glycol) (PEG), PVDF/sulfonated polystyrene, PVDF/poly(vinyl acetate) (PVA) [18], PVDF/poly(methacrylate) (PMA) [19], and PVDF/poly(methyl methacrylate) (PMMA) [9, 13, 20–24]. Among them, PVDF/PMMA is the most widely studied system in developing dielectric films due to their unique combination of good mechanical properties, excellent optical properties, high electrical resistivity, and good film casting processability.

W. Tang (✉) · P. Zhou
Key Laboratory of Soft Chemistry and Functional Materials, Nanjing University of Science and Technology, Nanjing 210094, People's Republic of China
e-mail: whtang@mail.njust.edu.cn

T. Zhu · W. Zhao · Q. Wang · G. Feng · H. Yuan (✉)
Key Laboratory of Beijing City on Preparation and Processing of Novel Polymer Materials, Beijing University of Chemical Technology, Beijing 100029, People's Republic of China
e-mail: yuanhuil@263.net

PMMA has been found to possess high compatibility with PVDF [21–24]. The addition of hydrophilic PMMA renders hydrophobic PVDF membrane with enhanced hydrophilicity and flux rate [25–27]. Zhang et al. studied the crystallization and surface morphology of PVDF/PMMA casting films from single or mixed solvents on different substrate [9, 13, 20]. The results show that PVDF exclusively from β-phase polymorph when casting from DMF solution onto substrates such as ceramic, polytetrafluoroethylene (PTFE), Cu, stainless steel, and glass substrates [20].

So far, all PVDF/PMMA studies focus on their solution-cast films, no information has been reported on the melt-mixed PVDF/PMMA blends and their blown films for encapsulation applications for Si-based solar cells. The objective of this research is thus to achieve the melt-blending PVDF/PMMA blends and the corresponding blown films. The crystallization, surface morphology and the hydrophilicity of the resulted blown films were studied. PVDF/PMMA/TiO_2 blown films were further prepared and followed with surface treatment to meet the demand of mechanical properties, adhesion capability, and reasonable hydrophilicity for solar cell encapsulation. PVDF/PMMA/TiO_2 blown films show attractive properties as encapsulation materials.

Experimental

Materials

PVDF powder (ATOFINA Co., France) has a melting point of 144 °C, decomposition temperature over 320 °C and melt flow index (MFI) of 4 g/10 min (at 230 °C under 12.5 kg load). PMMA (CM205, Chi Mei Co., Taiwan) has a MFI of 125 g/10 min (at 230 °C under 3.8 kg load). TiO_2 (R-350) was obtained from DuPont Co., USA. The silane coupling agent, 3-(triethoxysilyl)propan-1-amine (KH550), used for surface modification of TiO_2, was obtained from Dow Corning (Shanghai).

Blowing films prepared by extrusion

All blending was performed in single-screw BRABENDAR extruder (Germany, Φ30, $L/D = 25$) with a rotation speed of 30–45 r/min according to designed blends composition. The barrel temperature profile for all blending was 160–170–200–210–190 °C from the hopper to the die. The extrudates exiting from the extruder were pelletized and oven-dried. PMMA was oven-dried at 120 °C for 4–6 h and mixed with PVDF prior to blending for binary polymer blends. In the following sections, the binary polymer blends of PVDF and PMMA at different compositions are denoted as DFMA*ij*, where *i* and j are the weight portions of PVDF and PMMA, respectively. For example, DFMA91 indicates the polymer blends consisting of 90 wt% PVDF and 10 wt% PMMA. For TiO_2-filled composites, PVDF/PMMA/TiO_2, TiO_2 was firstly dried at 120 °C for 3 h before mixing with KH550 at 80 °C for 20 min in a stirred autoclave. The surface modified TiO_2 was cooled to room temperature and underwent melt-blending with oven-dried PMMA in single-screw extruder. The extrudates of PMMA/TiO_2 were further melt-mixed with PVDF by extrusion to prepare TiO_2-filled PVDF/PMMA/TiO_2 composites.

For film blowing, a film blowing die with an adjustable slit (100–1000 μm) was mounted to the above-mentioned extruder. The blown films (100 μm in thickness) were prepared by extrusion with a barrel temperature profile 160–170–200–220–200 °C from the feed to the die at a rotation speed of 30–45 r/min.

Blown films of DFMA73/TiO_2 were surface modified by corona discharge processing with high performance electronic impacting machine (Success, China). Both sides of films were corona discharged under 60 V applied voltage with a speed of 3 m/min.

DFMA73/TiO_2 blown films were also surface-grafted with acrylic acid (AA) under UV-irradiation. Blown films were soaked in anhydrous ethanol for 1 h and dried in 90 °C oven for 3 h to remove any impurity on the surface. Two concentrically rolled blown films (diameter, 10 cm) were cut and added with (AA) aqueous solution (0.05 g/mL) between them. After homogenously coating of acrylic acid on the surface, the rolled films were irradiated under 8 mW/cm^2 254 nm-UV light for 2 min. The surface-treated blown films were then soaked in 50 °C water bath for 6 h with water changed every 1 h to remove non-grafted poly(acrylic acid).

Instrumental analysis

Thermal analysis of DFMA films was performed in N_2 atmosphere on PerkinElmer differential scanning calorimeter with analysis temperature ranging from 50 to 430 °C at a heating rate of 10 °C/min. The crystalline structure of PVDF in PVDF/PMMA blends was investigated on an RIGAKU X-ray diffractometer (D/MAX2500VB2+/PC X, nickel-filtered Cu Kα radiation, 40 kV and 200 mA). The XRD spectra were recorded in the range of $2\theta = 5°$–$50°$ with a scanning rate of 5°/min and recorded every 0.05°. The surface morphology of DFMA films was observed with tapping mode atomic force microscope (AFM, EX-1, Metrology Group). FT-IR spectra were recorded on BRUKER TENSOR 27 FT-IR spectrometer to investigate the interaction between PVDF and PMMA along the film surface.

The tensile tests were performed on Instron universal tester (model 1185) according to GB13022-91 with a crosshead speed of 20 mm/min at 25 °C and 50% humidity. The morphology of the DFMA blends and DFMA/TiO_2 composites were examined using JSM-6360LV scanning electron microscope (SEM). The sheet specimens were extruded from BRABENDAR single crew extruder with temperature profile 160–250 °C and cryogenically fractured in liquid nitrogen. The samples were dried and sputter-coated with a thin layer of gold before examination with SEM. The surface microphotograph of surface-treated blown film and water contact experiments were observed with Olympus (BX51) optical microscope.

Water contact angle measurement

The surface hydrophilicity was studied by measuring the water contact angle for the blown films with varied compositions. The static water contact angles were measured using a telescopic goniometer (JC200C1, Shanghai Zhongchen digital technique equipment Co. Ltd, China) at 25 °C and 50% relative humidity. At least five specimens of each composition were tested and the average value was reported with an error below 5°.

Results and discussion

Thermal analysis

The miscibility of a blend including a semi-crystalline component like PVDF is generally realized by the interaction between amorphous parts of each component. When this interaction interrupts the crystallization of crystalline component, a melting point (T_m) depression of crystalline component (PVDF) occurs and thus can be used to estimate the interaction parameter B between two components [18], i.e., PVDF and PMMA in our case.

$$T_m^0 - T_m = -T_m^0 \frac{BV_{2u}}{\Delta H_{2u}} \Phi_1^2 \quad (1)$$

where T_m^0 and T_m are the equilibrium melting points of pure PVDF and PVDF in DFMA, respectively; the subscript 1 and 2 represent noncrystallizable component (PMMA) and crystallizable one (PVDF), respectively; Φ_1 is the volume fraction of PMMA in DFMA blend; and $\Delta H_{2u}/V_{2u}$ is the heat of fusion per unit volume of PVDF. PVDF has a $\Delta H_{2u}$of 1600 cal mol^{-1} and a V_{2u} of 36.4 cm^3 mol^{-1} [12]. When PVDF is blended with PMMA, its melting points suffer depression with increasing the content of amorphous PMMA, as DSC traces shown in Fig. 1. The fusion heat (area of the peak) of PVDF also reduces in DFMA blends with gradually increased content of PMMA, e.g., DFMA55. As a result, for all DFMA blends, since $T_m^0 - T_m$ is positive due to the depression of melting point, the interaction parameter B is always negative according to Eq. 1. The negative values of B indicate the miscibility of the blends with PVDF crystals immersed in the amorphous region of the matrix. It should be mentioned that the matrix is composed by both amorphous part of PVDF and all PMMA, since PVDF and PMMA are compatible [13]. This compatibility can be observed by SEM images of DFMA and DFMA/TiO_2 composite (Fig. 7).

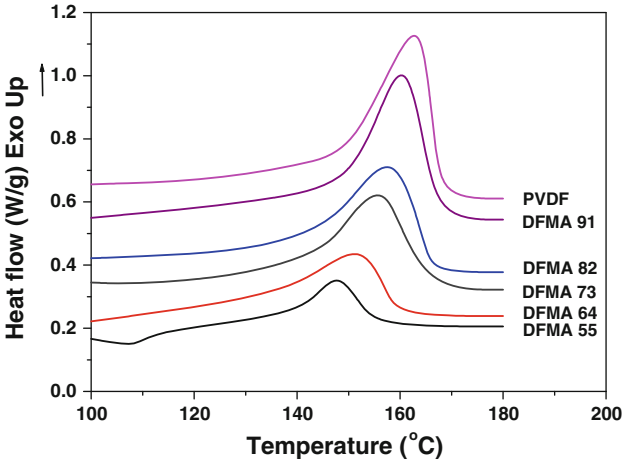

Fig. 1 DSC traces of PCDF and the blend films of DFMA with varied weight ratio of PVDF and PMMA

The broadening of PVDF melting range can also be observed for DFMA blends in Fig. 1. For instance, the pristine PVDF has a 10 °C melting range with an onset temperature at 155 °C and a final melting temperature at 165 °C; while DFMA82 shows a 25 °C melting range with the onset temperature decreased to 140 °C and unchanged final melting temperature. With PMMA content increasing up to 30 wt%, the onset melting temperature drops below 140 °C and final melting temperature remains at 162 °C. The area of melting peak (fusion heat) decreases obviously, indicating dramatic decrease of PVDF's crystallinity. With further addition of PMMA, the interruption of PVDF crystallization was intensified by the interaction between PMMA and PVDF. This can be explained by the structure difference between PVDF ($T_g = -50$ °C) and PMMA ($T_g = 125$ °C) [17]. The polymer chains of PVDF are more flexible than those of PMMA at melt state, the segments of PVDF can still move to crystallize with reasonable addition of PMMA. In most reported crystallization studies on solution-cast DFMA films, the crystallization of PVDF was retarded at total polymer solution concentration >5 wt%. The retardation is attributed to the limited space for crystallization, which is difficult for the motion of polymer chains [6, 28, 29]. Zhang et al. used semi-dilute solution (total polymer concentration = 2 wt%) to make more

space for chains' motion. In this dilute homogenous solution of PVDF and PMMA, polymer chains are overlapped and entangled with slow motion. Under this condition, β-form crystals dominate regardless of PMMA content. On the contrary, small addition of PMMA (10 wt%) promotes the crystallization of PVDF and induces larger lamellar thickness of PVDF spherulites. The crystallinity of PVDF decreased when further increasing content of PMMA [13]. In our case of blown films, the mixing of PVDF and PMMA is inferior to that in semi-dilute solution. Therefore, the interruption of the crystallization of PVDF is much more intensified by the addition of PMMA. As observed, the crystallinity of DFMA blown films decreases dramatically with the addition of PMMA.

X-ray diffractometry

The lower beam mode XRD was employed to detect the crystal structure near surface [12]. Figure 2 shows the XRD patterns of surface phase in DFMA films. The pristine PVDF has four characteristic peaks of α-phase PVDF appearing at $2\theta = 17.8°$, 18.2°, 20.0°, and 26.6°, attributed to the fraction at planes (100), (020), (110), and (021), respectively [28]. As shown, α-polymorph is prevailing in PVDF blown film, in good agreement with the literature about PVDF crystal structure obtained from melt [1]. The diffraction peak at $2\theta = 20.26°$ is assigned as the characteristic diffraction of β-phase PVDF in plane (110) [13]. With addition of PMMA, diffraction peaks for α-phase PVDF at planes (110) and (020) weakened, while the diffraction at plane (110) for β-phase PVDF intensified when comparing DFMA91, DFMA82, DFMA73, and DFMA64. The incorporation of PMMA into PVDF clearly induces the formation of β-phase PVDF, which is quite different to the solution-cast films [13]. In DMF solution-cast PVDF films, only β-phase diffraction peak at $2\theta = 20.26°$ appeared and this peak became weaker with the addition of PMMA [13]. It is worthy to note that in all blown films no diffraction peaks appeared at $2\theta = 22.8°$, characteristic of γ-phase PVDF at plane (111) [12]. With further increasing the content of amorphous PMMA in DFMA blends, e.g., DFMA64, the XRD pattern exhibits very weak diffractions, indicating an amorphously prevailing matrix exists in the near surface layer of blown film. This is in agreement with the crystallization of PVDF, which decreased with increasing content of PMMA.

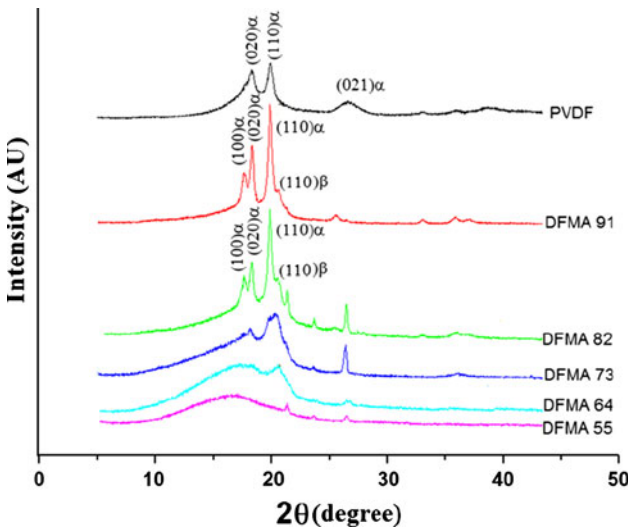

Fig. 2 XRD spectra of the surface phase of PVDF and DFMA films

Surface morphology

The surface morphology of blown films of PVDF and DFMA was observed with tapping mode AFM with scanning range limited within 1 μm, a size smaller than the dimension of a single crystal grain (Fig. 3). Therefore, local crystal structure can be detected with AFM imaging. Since α-polymorph monoclinic unit cells are dominant in our blown films, as revealed by the above-discussed XRD study. By sensing the change in phase angle of the cantilever probe, the phase contrast image can be achieved to distinguish different material phase in the film surface [30]. The AFM image of the pristine PVDF blown film pinpoints the fine crystal structure, which is observed as arrays of bright domains projecting outside of the coarse surface. In this typical hill-valley topography, the bright domains seem to be generated from orderly folding of long-range ordered PVDF segments, and the dark domains are likely formed due to the visco-elastic response of the random entanglement of segmental PVDF. Upon the introduction of PMMA, the film surfaces become smoother than that of pristine PVDF, mainly due to the decreased long-range ordered PVDF segments with decreased crystallinity. For instance, with addition of 10 wt% PMMA, the resulting DFMA91 film (Fig. 3a) exhibits a similar topography except for the increased smoothness and lowered height contrast. For DFMA28, similar topography still can be observed though its crystallinity decreases dramatically with 80 wt% PMMA. This is may be explained by the surface enrichment of PVDF segments in the surface, due to lower surface tension of PVDF than PMMA.

Hydrophilicity of DFMA films with addition of PMMA

The contact angle test was carried out on the smooth surface of DFMA blown films. The surface hydrophilicity for DFMA films changes with the addition of PMMA (Fig. 4). The curve of water contact angle versus the content of PVDF in DFMA films consists three sections. A plateau seems to exist for DFMA blends with PVDF content

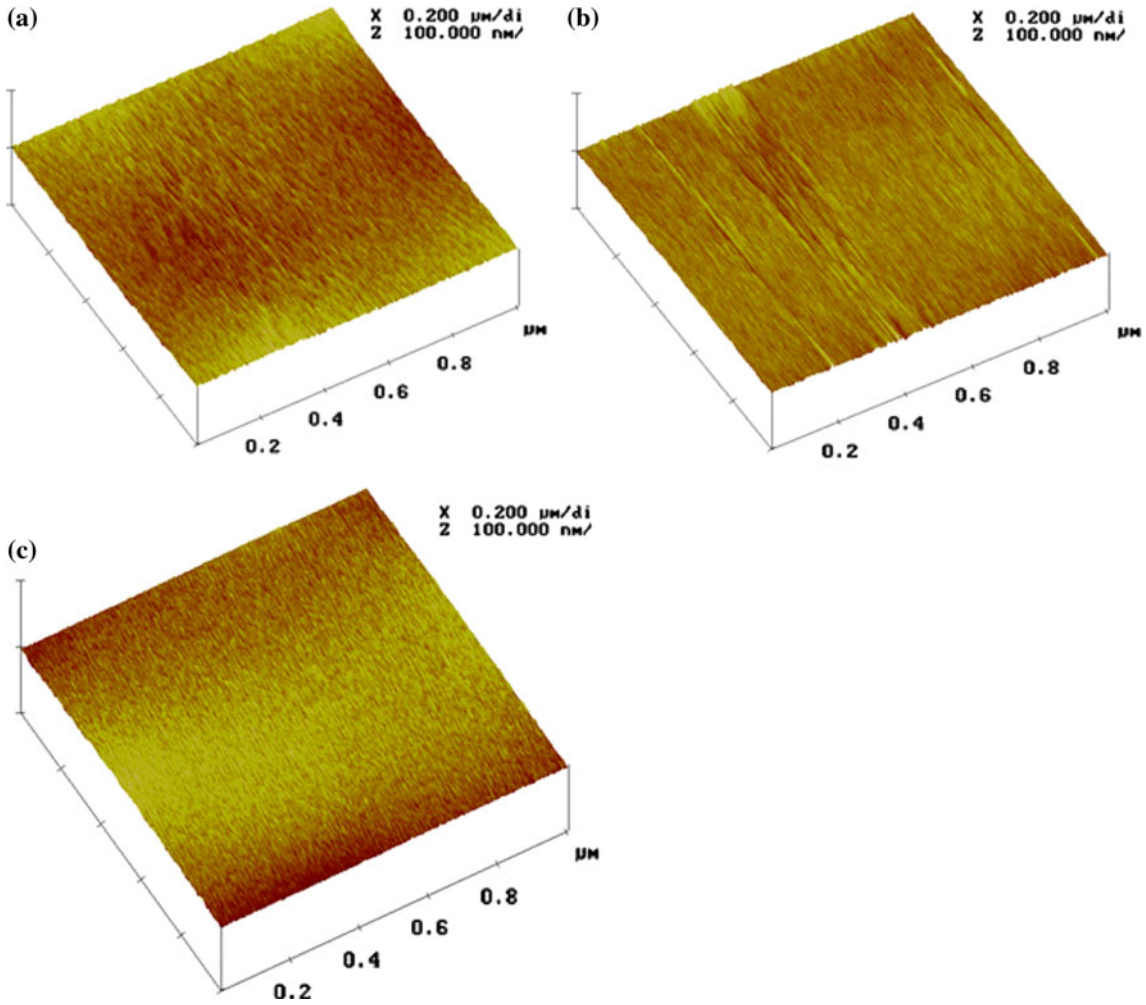

Fig. 3 AFM phase images of blown films of: **a** PVDF; **b** DFMA91; and **c** DFMA28

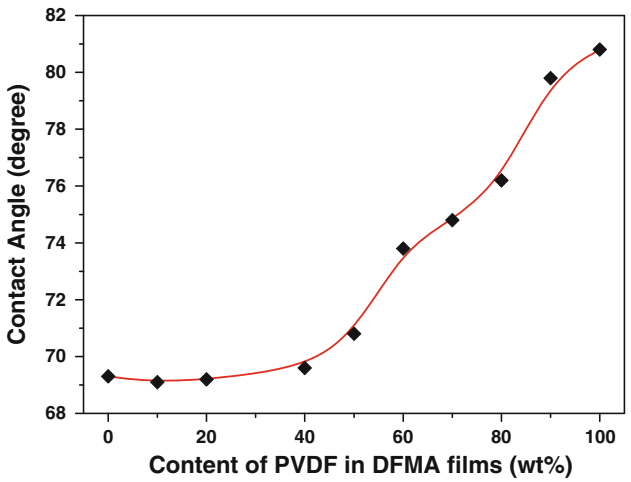

Fig. 4 The variation of water contact angle with PVDF content in DFMA films

ranging from 60 to 80 wt%. The similar plateau was also observed in PVDF/PVP solution-cast films with PVDF concentration in the range of 80–60 wt% [13]. The presence of plateau region indicates that the transformation processes occurring with an increase in PVDF content: (i) the resume of surface enrichment tendency to PVDF, and (ii) the contraction of PVDF crystalline domains on the film surface, with the former promoting the hydrophobicity of the surface while the later producing the opposite effect. Therefore, a hydrophobic–hydrophilic equilibrium is approximately maintained across this plateau. Prior to this equilibrium, the hydrophilicity of DFMA films changes slightly with PVDF content below 40 wt%. The contact angle against water is less than 70°, indicating a characteristic hydrophobic surface [31]. With PVDF content greater than 80 wt%, i.e., the section after the plateau shows increased hydrophobicity. The hydrophilicity change in DFMA blown films is in good agreement with that for solution-cast films [13].

Effect of TiO_2 filling on blown films

Based on the discussion above, DFMA73 shows a good combination of crystallinity, hydrophilicity, chemical resistance, hardness, mechanical strength, and weatherability [27]. DFMA73 are further employed in the preparation of DFMA73/TiO_2 blown films. TiO_2 has been extensively used as anti-reflection coating for its high-temperature stability (T_m = 1830–1850 °C) and high refractive index (n = 2.55–2.70) [32]. The incorporation of TiO_2 into DFMA blend film may improve its mechanical properties like tensile strength and resistance to discoloration under sunlight.

The mechanical properties of DFMA73/TiO_2 composite are listed in Table 1. As shown, 15 wt% addition of TiO_2 to DFMA73 does not make too much change to the mechanical properties of PVDF film. The composite harvests slight improvement in yield strength and tensile strength at the cost of little drop in elongation at break and tear strength. In comparison with the widely used PVF/TiO_2 protective film [33], DFMA73/TiO_2 films present similar yield strength and tensile strength, but much improved elongation at break and tear strength. This can be explained by the structure difference. PVF (polyvinyl fluoride) contains single fluorine atom in every repetition unit and is weaker to form hydrogen bonding with electronegative oxygen atoms than PVDF in DFMA73/TiO_2 blends. However, PVF displays higher elastic modulus than pristine PVDF and its composites.

The dispersion of TiO_2 in DFMA73 films with 5, 10, and 15 wt% TiO_2 addition was observed with SEM. As shown in Fig. 5, PVDF and PMMA are compatible to form a homogeneous matrix; TiO_2 particles (dimension up to 2 μm) well disperse in DFMA matrix to form the typical island-sea topography. It should note that TiO_2 particles suffer certain aggregation though TiO_2 nanoparticles were surface-treated with silane coupling agent (KH550). This aggregation maybe account for the slight change in the mechanical properties of DFMA films, since well-dispersed inorganic particles like alumina often result in large improvement in the tensile strength and elongation of PVDF [3]. Interestingly, the dimension and dispersion of TiO_2 particles remain almost unchanged with increased content of TiO_2, probably due to the anti-aggregation effect of the added coupling agent.

Comparison of surface morphology after surface modification

DFMA/TiO_2 blown films underwent further surface treatment with corona discharge and acrylic acid (AA) surface-grafting tailoring for ethylene vinyl acetate (EVA) encapsulation, with their surface morphology shown in Fig. 6. The pristine DFMA/TiO_2 film surface presents homogenous and relatively smooth topography (Fig. 6a). The corona-treated DFMA/TiO_2 film surface becomes coarser and displays obvious trace of ablation, with clear tiny speckles observed in the surface. These speckles were formed due to the bombardment of high-energy particles on the surface during corona discharge [34]. These speckles can act as the physical anchors for adhesion. However, overly corona-treated DFMA/TiO_2 films are found to be difficult for the following adhesion and soakage with ethylene vinyl acetate (EVA) sealant. On the

Table 1 Mechanic properties of DFMA/TiO_2 (15 wt%) blown films

Blown film	Yield strain (%)	Yield strength (Pa)	Tensile strength (Pa)	Elongation at break (%)	Elastic modulus (MPa)	Tear strength (N/m)
PVDF	3.79	5221	7196	235	174	602
DFMA73 + TiO_2	3.85	5270	7342	214	170	565
PVF + TiO_2	–	6000	8000	90	305	264

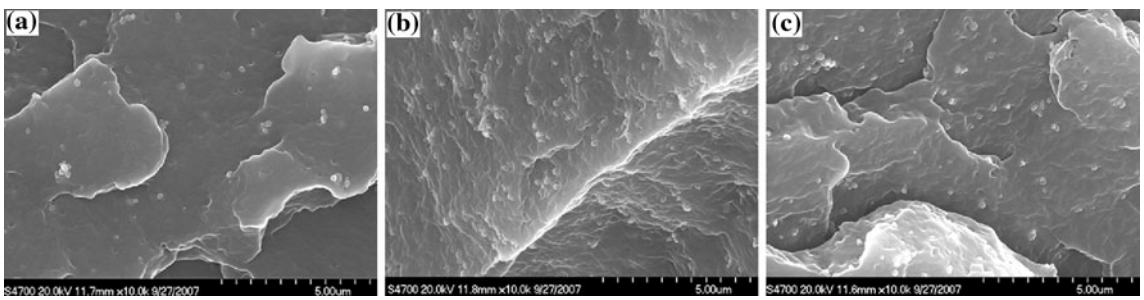

Fig. 5 SEM micrograph of cross-section of DFMA73/TiO_2 films: **a** 5 wt% TiO_2, **b** 10 wt% TiO_2, and **c** 15 wt% TiO_2

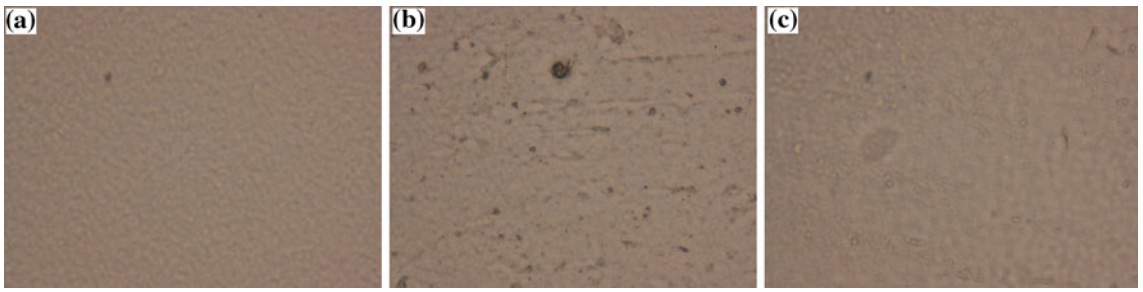

Fig. 6 Surface microphotographs for different films: **a** pristine DFMA73 film, **b** corona-treated DFMA73/TiO_2 film, and **c** acrylic acid surface-grafted DFMA73/TiO_2 film

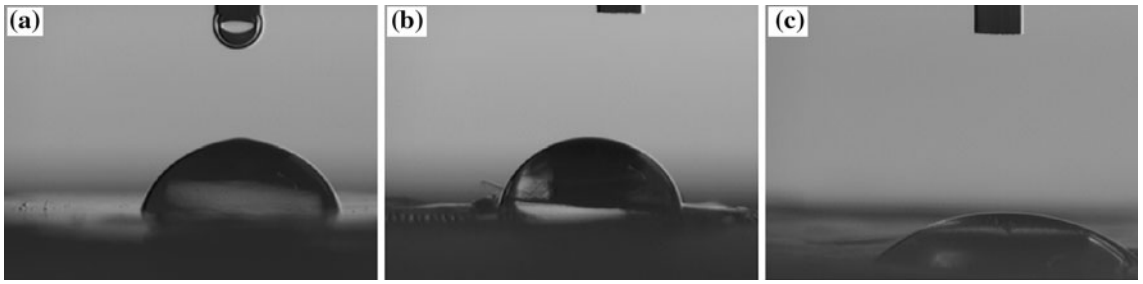

Fig. 7 Microphotographs of water dripping experiment on different film surface: **a** pristine DFMA73 film, **b** corona-treated DFMA73/TiO_2 film, and **c** acrylic acid surface-grafted DFMA73/TiO_2 film

other hand, UV light irradiated AA-grafted DFMA/TiO_2 film changes slightly except for coarser surface (Fig. 6c) in comparison with untreated blown film. The tearing experiments of heat-sealed DFMA/TiO_2 blown films with EVA thin layer reveal that AA-grafted DFMA/TiO_2 cannot be peeled off from EVA layer, due to chemical bonding, while corona discharged blown film is easy to be peeled off. The results indicate that AA surface-grafted DFMA/TiO_2 film is capable for adhesion with EVA sealant and thus applicable for encapsulation layer for solar cell panel.

Water dripping experiment on the film surface

The hydrophilicity of the surface-treated DFMA/TiO_2 films was further demonstrated with water dripping experiment. Figure 7 shows the improvement of hydrophilicity for both corona-treated and irradiation-induced acrylic acid grafted film surface, with the latter superior to the former approach. The time-dependant hydrophilicity was also explored for different surface treatment approach. The results show that corona-treated films remained its hydrophilicity within the first 24 h and almost lost its effectiveness after 15 days, which may be explained by the low PVDF's concentration in the surface. On the contrary, via chemical bonding onto DFMA surface, AA surface-grafting blown films achieved significantly increased hydrophilicity (Fig. 7c). More importantly, the enhanced hydrophilicity does not change at wall in the time-window in our study.

In summary, AA surface-grafted DFMA/TiO_2 films present good balance of mechanical properties, surface adhesion capability, and hydrophilicity, which is thus attractive for the application as encapsulation layer for solar cell panel.

Conclusions

PVDF/PMMA blown films were firstly achieved by melt extrusion. The crystallization behavior, surface morphology, and hydrophilicity of this blown film were studied in detail using DSC, XRD, and AFM. The results show that PVDF and PMMA have good compatibility with the formation of quasi-hydrogen bonding. α-polymorph PVDF dominates in blown film while β-polymorph can be induced by the addition of PMMA. PVDF/PMMA/TiO_2 blown films were further prepared, with mechanical properties, adhesion capability, hydrophilicity systematically investigated. The irradiation-induced AA surface-grafted DFMA blown films present a good combination of mechanical properties, adhesion capability, and reasonable hydrophilicity.

Acknowledgements This work was partially supported by Nanjing University of Science and Technology. The authors acknowledge the financial support from Foundation of Key Laboratory of

Luminescence and Optical Information (2010LOI04), and NUST Research Funding (NO. 2010ZDJH04).

References

1. Matras-Postolek M, Bogdal D (2010) Adv Polym Sci 230:221
2. Hietala S, Holmberg S, Karjalainen M, Paronen M, Serimaa R, Sundholm F, Vahvaselkä S (1997) J Mater Chem 7:721
3. He F, Fan J, Lau S (2008) Polym Test 27:964
4. Mawson S, Johnston KP, Combes JR, DeSimone JM (1995) Macromolecules 28:3182
5. Scheinbeim JI (1999) In: Mark JE (ed) Poly(vinylidene fluoride). Oxford University Press Inc, New York
6. Gregorio R Jr, Cestari M (1994) J Polym Sci B 32:859
7. Tazaki M, Wada R, Okabe M, Homma T (1997) J Appl Polym Sci 65:1517
8. Cheng LP (1999) Macromolecules 32:6668
9. Salimi A, Yousefi AA (2004) J Polym Sci B 42:3487
10. Hsu CC, Geil PH (1989) J Mater Sci 24:1219. doi:10.1007/BF02397050
11. Botelho G, Lanceros-Mendez S, Gonçalves AM, Sencadas V, Rocha JG (2008) J Non Cryst Solids 354:72
12. Chen N, Hong L (2002) Polymer 43:1429
13. Ma W, Zhang J, Wang X, Wang S (2007) Appl Surf Sci 253:8377
14. Alfonso GC, Turturro A, Pizzoli M, Scandola M, Ceccorulli G (1989) J Polym Sci B 27:1195
15. Kammer H-W, Macromol J, Sci A (1990) Pure Appl Chem 27:1713
16. Yang HH, Han CD, Kim JK (1994) Polymer 35:1503
17. Nunes SP, Peinemann KV (2001) In: Nunes SP, Peinemann KV (eds) Membrane technology in the chemical industry. Wiley–VCH, Weinhein
18. Lee WK, Ha CS (1998) Polymer 39:7131
19. Pralay M, Nandi AK (1998) Polymer 39:413
20. Ma W, Zhang J, Wang X (2008) Appl Surf Sci 254:2947
21. Sasaki H, Bala KP, Yoshida H, lto E (1995) Polymer 36:4805
22. Roerdink E, Challa G (1978) Polymer 19:173
23. Hourston DJ, Hughes ID (1977) Polymer 18:1175
24. Hang C, Zhang L (2004) J Appl Polym Sci 92:1
25. Nunes SP, Peinemann KV (1992) J Memb Sci 73:25
26. Ochoa NA, Masuelli M, Marchese J (2003) J Memb Sci 226:203
27. Lin SC, Argasinski K (1999) In: Hougham G, Cassidy PE, Johns K, Davidson T (eds) Fluoropolymer alloys performance optimization of PVDF alloys. Plenum Press, New York
28. Gregorio R Jr (2006) J Appl Polym Sci 100:3272
29. Rocha IS, Mattoso LHC, Malmonge LF, Gregório R Jr (1999) J Polym Sci B 37:1219
30. Raghavan D, Gu X, Nguyen T, Van Landingham M, Karim A (2000) Macromolecules 33:2573
31. Adachi S, Arai T, Kobayashi K (1996) J Appl Phys 80:5422
32. Richards BS (2004) Prog Photovolt Res Appl 12:253
33. Pern FJ, Glick SH (2000) Sol Energy Mater Sol Cells 61:153
34. Iwata H, Kishida A, Suzuki M, Hata Y, Ikada Y (1988) J Polym Sci A 26:3309